Uichung Cho
Senior Engineering Manager,
LG Electronics,
7105 Teya Court,
Austin, TX 78749
e-mail: francisu@lge.com

Alan J. Dutson
Brigham Young University–Idaho,
159 H. Austin Building,
Rexburg, ID 83460
e-mail: dutsona@byui.edu

Kristin L. Wood
Professor,
University of Texas,
ETC 4.146B,
Austin, TX 78712
e-mail: wood@mail.utexas.edu

Richard H. Crawford
Professor,
University of Texas,
ETC 4.116,
Austin TX 78712
e-mail: rhc@mail.utexas.edu

An Advanced Method to Correlate Scale Models With Distorted Configurations

Functional testing of prototypes is a critical step in the development of many of today's products. Results of functional tests allow for verification of proper performance before a product is introduced into the market. The advent of rapid prototyping technologies offers engineers the potential to dramatically reduce the prototype-test-verify cycle and get products to market quickly. However, dimensional and material property limitations of rapid prototypes often prevent them from being used for functional testing without the use of similitude methods to correlate measured prototype behavior with predicted product behavior. The traditional similarity method (TSM), which is based on the Buckingham Π *theorem, requires that the dimensionless parameters of the prototype and product systems be identical in order to correlate their states and accurately predict product performance. The requirement of identical dimensionless parameters which is inherent in the TSM is often impossible to realize with the limited properties available from rapid prototyping technologies. In order to overcome this limitation, an empirical similarity method (ESM) has been developed. The general concept of the ESM is introduced along with an implementation procedure. Numerical and experimental examples are presented which demonstrate the feasibility and industrial impact of the ESM in the context of product design.* [DOI: 10.1115/1.1825044]

Background

Product design and development processes recursively synthesize products that satisfy customer needs and functional requirements within limited temporal and financial resources [1–3]. Companies continuously collect and analyze functional, aesthetic, ergonomic, and manufacturing information to produce quality products. The effort required to obtain such information is one of the key factors that determines the performance of the design process [4,5,3].

Various types of virtual and physical models are utilized to provide proper functional information for a product. Virtual models are preferred to physical models in many cases because of their high flexibility, short development time, and relatively low cost. Despite significant advances in virtual modeling, however, the natural phenomena that can be accurately and confidently represented purely by virtual models are still very limited. Thus, companies typically utilize both virtual and physical models to verify and refine product designs.

During the last two decades various rapid prototyping techniques have been developed which produce geometrically complex physical models with significantly reduced fabrication effort [6,7].[1] Considering the significant time and cost spent on product testing, it is natural to expect various industrial applications of rapid prototypes for functional testing. However, companies appear to utilize rapid prototypes mostly in the early design stages. Very few case studies are reported on functional testing with rapid prototypes [8–10], with material limitations being a key factor [11]. Similarity methods represent an opportunity to overcome these limitations and advance the state-of-the-art.

There exist primarily two types of similarity methods that correlate scaled prototypes and full-scale products: (1) the Buckingham Π theorem approach that correlates scaled model and product behaviors by considering dimensions of dominant system parameters [12–16]; and (2) an analytical approach that mathematically correlates the solutions of two known equations by comparing and manipulating the equations [14,17,18]. The analytical approach can provide accurate scale testing results in general [18] but has limited application since it requires *a priori* knowledge of the governing equations for the system. The Buckingham Π approach (also know as dimensional analysis or the traditional similarity method, TSM) has a much wider range of application and is the approach considered in this paper.

The concept of the TSM and its inherent limitations can be understood by considering the mathematical foundations of the method. Consider two systems (a model[2] and a product) whose behavior can be represented with the following complete equations:

$$f(d_{m,1}, d_{m,2}, \ldots, d_{m,n}) = 0,$$
$$f(d_{p,1}, d_{p,2}, \ldots, d_{p,n}) = 0, \tag{1}$$

where the subscripts m and p denote the model and the product respectively, and d_j is a system design parameter. The Buckingham Π theorem [12] states that a complete equation written in terms of dimensional system parameters d_j, $j=1,\ldots,n$, can be recast in terms of dimensionless parameters π_i, $i=1,\ldots,N$, where $N<n$. By applying the Π theorem, the above system of equations can be equivalently represented as

$$F(\pi_{m,1}, \pi_{m,2}, \ldots, \pi_{m,N}) = 0,$$
$$F(\pi_{p,1}, \pi_{p,2}, \ldots, \pi_{p,N}) = 0, \tag{2}$$

where $N=n-k$, and k is equal to or less than the number of fundamental dimensions [12,16]. Each dimensionless parameter π_i is a power function of the system parameter set $D=\{d_1, d_2, \ldots, d_n\}$. One can refer to [19] for a systematic derivation of the dimensionless parameters.

Contributed by the Design Theory and Methodology Committee for publication in the JOURNAL OF MECHANICAL DESIGN. Manuscript received September 11, 2003; revised April 22, 2004. Associate Editor: L. C. Schmidt.

[1]Material adapted from a paper presented at the 1999 ASME DETC Conference, Sept. 12–15, Las Vegas, NV, titled "System-Level Functional Testing for Scaled Protoypes with Configurational Distortions" by U. Cho, K. Wood, and R. Crawford.

[2]The term *model* will be used throughout the remainder of this paper to refer to a scaled replica of a product.

The dimensionless parameters that contain the state of interest of the two systems, say X_m and X_p, can now be described explicitly in terms of the other dimensionless parameters as

$$\pi_{m,X} = g(\pi_{m,1}, \pi_{m,2}, \ldots, \pi_{m,N-1}),$$
$$\pi_{p,X} = g(\pi_{p,1}, \pi_{p,2}, \ldots, \pi_{p,N-1}). \tag{3}$$

From Eq. (3), one can perceive that $\pi_{m,X}$ and $\pi_{p,X}$ are identical, if $\pi_{m,i} = \pi_{p,i}$ for all $i = 1,2,\ldots,N-1$. As a consequence, one can correlate the model and product states from

$$\pi_{p,X}(\mathrm{D}_p) = \pi_{m,X}(\mathrm{D}_m), \tag{4}$$

if

$$\pi_{p,i}(\mathrm{D}_p) = \pi_{m,i}(\mathrm{D}_m), \quad \forall i = 1,2,\ldots,N-1. \tag{5}$$

Equation (4), referred to as the *prediction equation*, and Eq. (5), called the *similarity constraints*, form the fundamental basis of the TSM. In order to predict a product state through the prediction equation, one should design a model so as not to violate any of the similarity constraints. If a model satisfies all similarity constraints, it is said to be *well-scaled*; otherwise, it is said to be *distorted*.

The assumptions of the TSM are that (1) the governing functions of the model and the product are identical; and (2) one can prepare a model that satisfies all of the similarity constraints. These assumptions may be violated, however, especially when models are fabricated from a rapid prototyping process. For example, two states X_m and X_p are not governed by the same function f if they have orthotropic and isotropic material structures, respectively, or if they exhibit nonlinear and linear behavior, respectively. In addition, similarity constraints become difficult to satisfy when available prototyping materials and achievable part sizes are limited. In these situations the model becomes distorted and scale testing results are not reliable. An additional source of error in the TSM is the omission of relevant system parameters, which causes the prediction equation to be incomplete. Such problems with the TSM have caused the reliability of scale testing results to be challenged frequently [16], forcing companies to rely on full-scale product testing instead of more economical prototype testing.

Due to the critical limitations of the TSM to perform reliable functional tests with rapid prototypes, an empirical similarity method (ESM) has been developed. The general concept of the ESM is presented in this paper along with applications of the method to problems with distorted configurations. The two examples used to illustrate the approach include an archery bow product and a CPU heat sink. The examples demonstrate the feasibility and potential industrial impact of the ESM in the context of product development.

Empirical Similarity Method

The goal of the ESM is to empirically derive more reliable correlations of models and products than is possible with the TSM by utilizing geometrically simple physical objects called specimens. The general concepts of the ESM are described in this section along with a procedure for using the method to perform system-level functional tests.

Historical Perspectives and General Concepts. Since Rayleigh's initial concept of dimensional analysis in 1915 [12], the TSM has been recognized as a simple but powerful tool to correlate systems and simplify experimental modeling tasks. Even though several cases show that dimensional information alone is not sufficient to correlate systems, no systematic method has been developed that can replace or significantly improve the TSM.

The TSM is a specific approach that constrains models such that product states can be predicted by multiplying the measured model states by a constant scale factor. If the constraints on the model are relaxed, the state relationship of the two systems is no longer a constant scale factor. Murphy showed, however, that there still may exist a consistent functional relationship between the model and product states, even though the constraints imposed by the Π theorem are not fully satisfied [20]. Similarly, Bluman and Kumei mathematically demonstrated that dimensional analysis is a special-case method to correlate systems [18]. They applied Sorphus Lie's group transformation to correlate different types of boundary and initial value problems. In spite of such research efforts, however, engineers still rely on the TSM since methods for deriving reliable correlations for general similarity problems, without the use of sophisticated mathematical models, are not available.

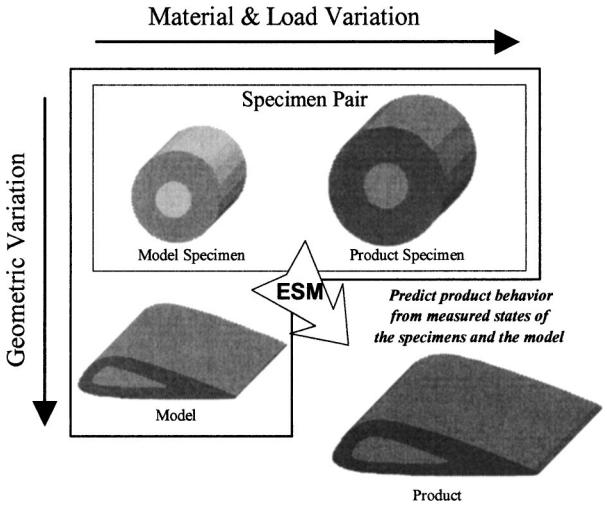

Fig. 1 Fundamental terms and concept of the ESM

Unlike existing methods that attempt to correlate systems based on dimensional information and analytical models, the ESM employs an additional pair of physical specimens to empirically correlate systems. The model specimen and product specimen are geometrically simplified versions of the model and the product, respectively. The basic concept of the ESM, in which the product state is predicted by measuring the states of the specimen pair (the model specimen and the product specimen) and the model, is shown in Fig. 1. The ESM assumes that

1. The state variation under purely geometric changes can be abstracted from the measured states of the model specimen and the model.
2. The state variation under purely nongeometric (material and loads) changes can be abstracted from the measured states of the model specimen and the product specimen.

Figure 2 further illustrates the basic premise of the ESM. The product is any part whose behavior is to be determined but which

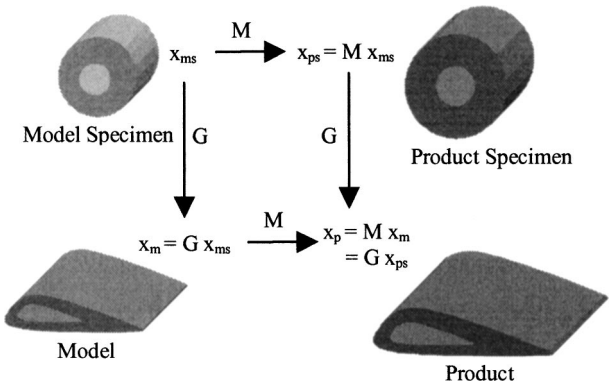

Fig. 2 Transformations used in the ESM

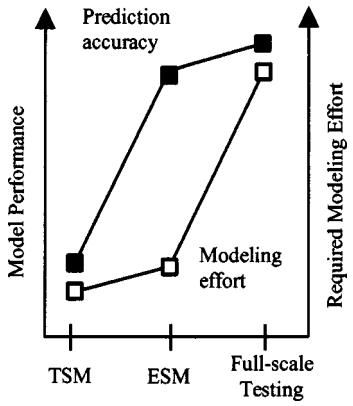

Fig. 3 Expected relative performance of the ESM

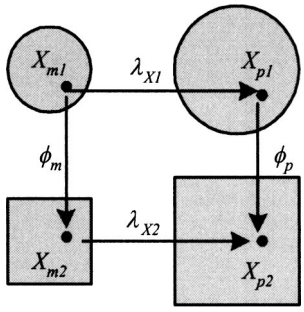

Fig. 4 Relationship between scale and form factors

contains complex geometry that is difficult to fabricate. The product specimen is a geometrically simplified version of the product which is made from the same material and processes as those for the product. The model is a geometrically equivalent version of the product which is made from a different material and process (e.g., a rapid prototyping process). The model specimen is a geometrically simplified version of the model which is made from the same material and process as the model. In Fig. 2, *G* represents the state variation under pure geometric changes, while *M* represents the state variation under pure material and loading changes. By constructing and testing the model, the model specimen, and the product specimen, both *M* and *G* can be determined and used to predict the state of the product. A detailed development of this ESM approach, along with specific examples of how the method can be implemented in product design, is presented later in the paper.

In designing the product specimen, basic geometric features are maintained (such as the existence of a hole) while the specific shape of such features are modified in order to simplify the fabrication process. Figure 2 illustrates one possible design for the specimen pair, although other possibilities definitely exist (e.g., triangular shape with a hole in the center). The specific shape of the specimen pair is not critical as long as the basic ESM assumptions discussed previously are met.

The ESM requires more preparation than the TSM since a specimen pair must be fabricated and tested. The additional effort, however, is still much smaller than that required to make full-scale prototypes for geometrically complex products. Wall showed that geometrical complexity is a critical factor in determining fabrication cost and time in traditional manufacturing processes (e.g., molding, machining, die casting, etc.) but not in rapid prototyping [11]. The objective of the ESM is clarified in Fig. 3 which qualitatively depicts the expected testing accuracy and required modeling effort of the ESM in comparison to full-scale testing and the TSM. As shown in the figure, the ESM attempts to attain highly accurate scale testing results at a fraction of the cost and time required for direct product testing, while recognizing that the ESM requires slightly more effort than the TSM.

The following sections detail an approach for representing the product state X_p as a function of measured states of the model (X_m) and specimen pair (X_{ms} and X_{ps}). Particular emphasis is given to systems composed of multiple parts.

Correlating Systems With Distorted Configurations—Lumped ESM. When products are composed of multiple parts, the TSM requires the design of models to satisfy the following material proportionality condition:

Proportionality of material properties—The material property ratio of the corresponding model and product parts should be kept identical in order to perform scale testing with the TSM.

The proportionality condition is very difficult to satisfy when available prototyping materials are limited. If two systems do not satisfy this proportionality, they are defined as having distorted configurations. A method to correlate systems with distorted configurations was not found within the reviewed literature. The lumped ESM has been developed to correlate distorted systems composed of more than one part.

Referring to Fig. 4, the ESM relates the state of a product (X_{p2}) to the states of the model (X_{m2}), product specimen (X_{p1}), and model specimen (X_{m1}) through scale and form factors. Note that the form factors and scale factors should satisfy

$$\lambda_{X1} \times \phi_p = \lambda_{X2} \times \phi_m, \tag{6}$$

where the scale factors λ_{X1} and λ_{X2} can be mathematically derived through dimensional analysis, and the form factors ϕ_m and ϕ_p are unknown. The form factors ϕ_m and ϕ_p, which represent the change in the model and product states that results from purely geometrical changes, should be identical if $\lambda_{X1} = \lambda_{X2}$, i.e., the model and the model specimen are designed from the same similarity constraints.

In the lumped ESM, each part is designed following the Π theorem in order to maintain identical scale factors ($\lambda_{X1}, \lambda_{X2}$) and, therefore, identical form factors (ϕ_{ms}, ϕ_p). The lumped model of the product specimen, the model, and the product can then be represented in terms of the model specimen parameters. This relationship can be manipulated to describe the state of the product as a function of the state of the model and the states of the specimen pair. The step-by-step procedure of this lumped ESM is summarized below.

Procedure for the Lumped ESM.

1. Build lumped parameter models: Describe the states of the model pair (the model and the model specimen) and the product pair (the product and the product specimen) as lumped models with unknown effective lumped parameters.
2. Determine the scale factor for each component: Design models through dimensional analysis and determine the scale factors of the lumped parameters (the ratio of the product parameter to the model parameter).
3. Describe lumped models relative to the model specimen: Employing scale factors and form factors, describe the model, the product specimen, and the product in terms of the model specimen. For example, a lumped parameter of a product C_p may be represented as $C_p(C_{\mathrm{ns}}, \phi, \lambda)$, where C_{ms} is a lumped parameter of the model specimen, λ is a scale factor that represents the variation of C_{ms} from changes in material properties and boundary conditions, and ϕ is a form factor that represents the variation of C_{ms} due to purely geometric changes. It should be noted that the factors λ and ϕ are assumed to be independent.
4. Represent product states in terms of the model and specimen states: By comparing and manipulating the four lumped models that are developed in the previous step, describe the

unknown product state as a function of the measured state of the model and the specimen pair, i.e. $X_p = f(X_m, X_{ms}, X_{ps})$.

In summary, the lumped ESM predicts a product state X_p by using the measured states of the specimen pair and the model. In general the number of unknown lumped parameters and form factors should be less than the number of measured states in order to solve for the product state in terms of known (measured) values. If the number of unknowns is greater than the number of equations, then a different set of boundary conditions may be applied to increase the number of equations (as demonstrated in the heat sink example), or component-level tests may be performed to determine form factors and reduce the number of unknowns.

Numerical and Experimental Examples

An archery bow (numerical) example and a heat sink (experimental) application are provided to illustrate the ESM approach. The selected examples demonstrate the wide range of application of the ESM in practical engineering problems. Each example also highlights difficulties in the TSM that are overcome by using the ESM.

Archery Bow Example. In designing archery bows, the shooting force, i.e., the force required to fully deform a bow to a shooting position, is a critical system behavior that can be predicted through prototype testing. Archery bows should be designed so that both ergonomic (e.g., required shooting force) and functional (e.g., arrow speed at a distance) requirements are satisfied. Although prototype testing and similitude can be used to predict the shooting force of a bow, geometric and material nonlinearities will likely cause errors in predictions made with the TSM. In addition, the geometric complexity of the bow frame makes fabrication of the test bows difficult and costly. In this example we demonstrate how a model bow can be used with the lumped ESM to predict the shooting force of a product bow. We also compare the ESM results with TSM results to demonstrate the improved prediction accuracy of the ESM.

This application of the lumped ESM is demonstrated using numerically simulated bow behaviors. Shooting forces were simulated with ANSYS™ finite element software. The finite element models of the target bows (product and model) and specimen bows are shown in Fig. 5. Note that the geometry of the specimen model has been simplified by approximating the curved section of the bow frame as a straight section. The string is modeled as a two-dimensional elastic link (Spar element), and the bow frame is modeled with triangular solid elements (Plane2). The width of the bow frame is 35 mm, and the cross section area of the string is 10 mm^2. The same bow string is used for both the model and the product bows. Parameters used in the finite element model are shown in Table 1. In this simulation, full-size models are used for the purpose of clear comparison. However, the size of the model bows can be reduced without loss of generality as long as the model systems are designed from the same scale laws.

Table 1 System parameters of the bows

Parameters	Model system (polymer bows)	Product system (fiber bows)
Frame E^b (GN/m^2)	7.46 (mean)	16.0 (constant)
String E^s (GN/m^2)	5	5
String prestrain	1E-8	1E-8

To predict the required shooting force of the target bow (product) through the ESM, it is assumed that both the model bow and the product bow can be represented as a lumped spring system, as shown in Fig. 6. The shooting force of a model specimen (polymer bow with the simple geometry shown in Fig. 5(*a*)) can then be described by the following equation:

$$F_{ms} = \frac{k^b_{ms} \times k^s}{k^b_{ms} + k^s} \delta, \tag{7}$$

where F is the shooting force, δ is the deflection of the bow string, and k^b and k^s are unknown effective spring constants of the bow frame and string respectively. By defining a state variable X, the force equation can be equivalently represented as

$$X_{ms} = \frac{\delta}{F_{ms}} = C^b_{ms} + C^s, \tag{8}$$

where $C^b = 1/k^b$ and $C^s = 1/k^s$ represent the effective compliances of the bow frame and string, respectively. Now the states of the product specimen, model, and product bows can be represented as

$$\begin{aligned} X_{ps} &= \lambda_c C^b_{ms} + C^s, \\ X_m &= \phi C^b_{ms} + C^s, \\ X_p &= \lambda_c \phi C^b_{ms} + C^s, \end{aligned} \tag{9}$$

where $\lambda_c = C^b_p / C^b_m = C^b_{ps} / C^b_{ms}$ is the compliance scale factor and $\phi = C^b_p / C^b_{ps} = C^b_m / C^b_{ms}$ is an unknown form factor of the bow frame. Note that the scale factor and form factor for the C^s term are both unity for this special case in which the same string is used for all systems.

The remaining task is to express X_p as $X_p = h(X_m, X_{ms}, X_{ps})$ so that we can predict X_p from the measured (or, in this case, simulated) states, X_m, X_{ms}, and X_{ps}, as illustrated in Fig. 1. From Eqs. (8) and (9), we can derive the following equations that eliminate the string-related parameters:

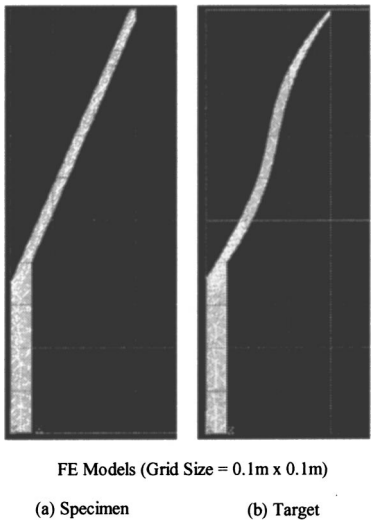

Fig. 5 Symmetric half of the specimen and product bows

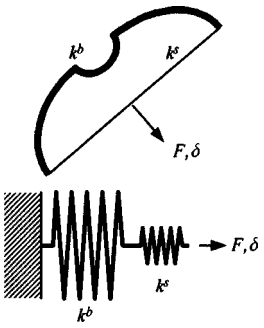

Fig. 6 Lumped model of a bow

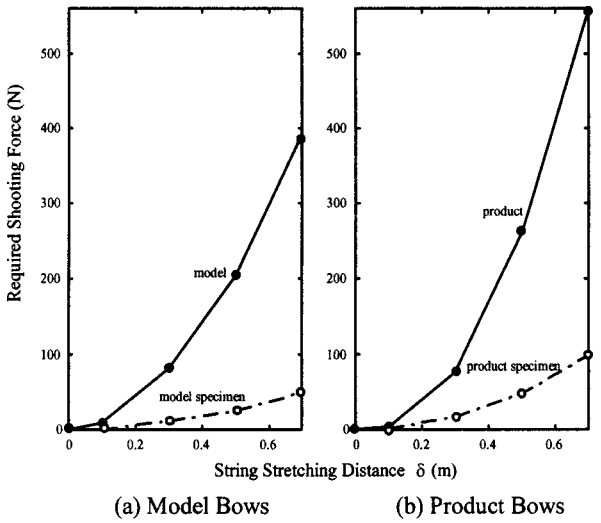

Fig. 7 Simulated shooting forces of the bows

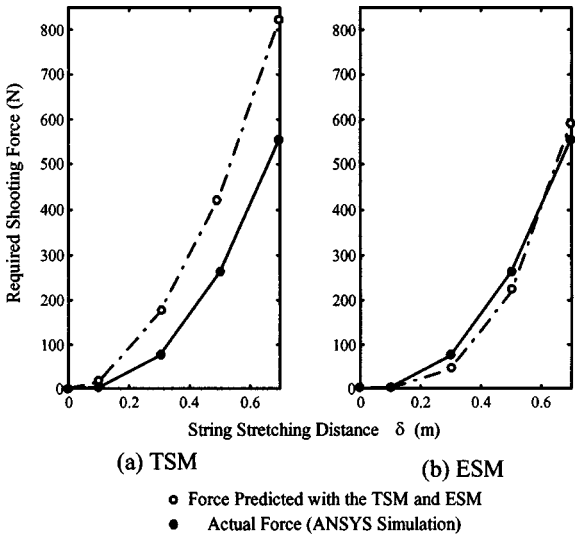

Fig. 8 Prediction of the shooting force with the TSM and ESM

$$X_p - X_{\text{ps}} = \lambda_c(\phi - 1)C^b_{\text{ms}},$$
$$X_m - X_{\text{ms}} = (\phi - 1)C^b_{\text{ms}}. \tag{10}$$

Combining the equations in Eq. (10) eliminates the unknown form factor ϕ and gives the prediction equation as

$$X_p = \lambda_c(X_m - X_{\text{ms}}) + X_{\text{ps}}, \tag{11}$$

where

$$\lambda_c = \frac{1}{\lambda_k} = \frac{E_m}{E_p}, \tag{12}$$

as determined from dimensional analysis for equal-sized bows. Now $X_p(\delta)$ can be predicted from the measured $X(\delta)$ of the specimens and the model (as shown in Eq. (11)) and the bow force $F_p(\delta)$ can be determined from the definition of the state X (as shown in Eq. (8)). Equation (11) represents the prediction equation for the ESM. A TSM prediction equation can also be created in order to compare ESM results with TSM. One way to perform scale testing with the TSM is to assume that the influence of the bow string on the reaction force is relatively small in comparison to the bow frame. In that case, dimensional analysis shows that, for bows of equal size, the ratio of the reaction force should be $F_p/F_m = E^b_p/E^b_m$ (see also [13]). Using values from Table 1 we have

$$F_p = \frac{16}{7.46}F_m = 2.14F_m. \tag{13}$$

Equation (13) is the prediction equation for the TSM.

The shooting force in all four bow systems (product, model, product specimen, and model specimen) was simulated with ANSYS™ for different values of deflection. Results are shown in Fig. 7. The nonlinear results in Fig. 7 are due to the nonlinear nature of the problem, as captured by the finite element solution. The simulation results for the model, model specimen, and product specimen are used with Eqs. (11) and (8) to predict the force in the product bow with the ESM. Simulation results for the model are used with Eq. (13) to predict the force in the product bow with the TSM. The simulated force for the product bow is considered to be the ''actual'' force and is used to compare the ESM and TSM predictions. Figures 8(*a*) and 8(*b*) show the shooting force predicted through the TSM and ESM, respectively, as compared with the actual shooting force. As shown in the figure, the error in the TSM prediction increases as the deflection increases (with a maximum prediction error of approximately 250 N), while the error in the ESM prediction remains relatively low across the entire range of deflection (with a maximum prediction error of approximately 30 N).

Figure 9 shows the resultant force ratio F_p/F_m which should be 2.14 in the ideal case for TSM (Eq. (13)). The difficulty in predicting product bow forces through the TSM can be perceived by noticing the variation of the resultant state scale factor (F_p/F_m) with respect to the applied displacement. The bow force predicted through the lumped ESM, however, shows remarkably improved prediction accuracy. Note that ESM prediction error does exist in Fig. 8(*b*), but is relatively small. Geometric nonlinearity of the bow frame due to the large deflection is probably the main cause of the error.

Heat Sink Application. Proper control of the steady state temperature of CPU surfaces is critical to CPU performance. For example, Intel recommends that the center of the Pentium II CPU processor be kept below 65°C. The surface of the Pentium II processor can reach up to 150°C without cooling. In addition, an advanced chip mounting technology (single edge connector) has been employed for more compact component mounting in which the mass of the CPU and its cooling system should be less than 105 g [21]. The requirement for effective heat dissipation, coupled with the constraint that the overall system mass must be 105 g or less, makes the design of CPU heat sinks a challenging problem.

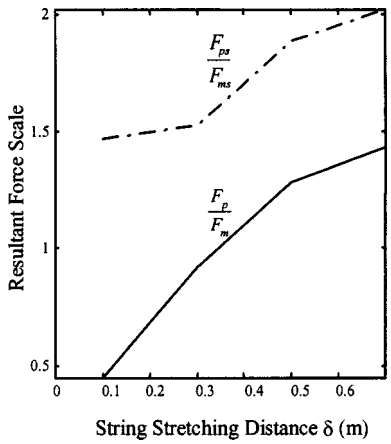

Fig. 9 Simulated shooting force ratios

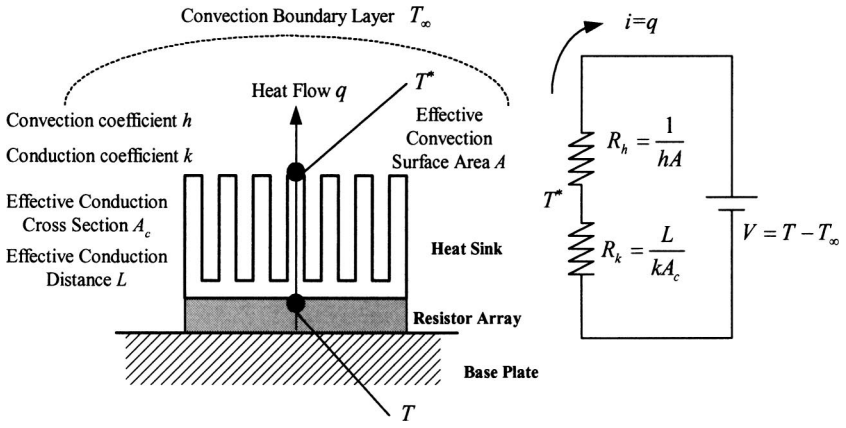

Fig. 10 Lumped model and equivalent electric circuit of heat sink systems

Virtual modeling of the steady-state temperature of thermal systems, which are composed of a CPU, a heat sink, and a cooling fan to circulate heated air, still needs improvement [22,23]. Virtual modeling of the CPU cooling process requires complex computational fluid dynamics (CFD). One problem in CFD modeling is the fact that including detailed geometry creates a model of unmanageable size [24]. In this subsection, we examine the feasibility of performing CPU cooling tests with polymer heat sinks fabricated with a rapid prototyping technique called selective laser sintering (SLS) [6,25,26]. The heat sinks were produced from DuraForm[3]. Results of the tests are used with the ESM to predict the performance of the actual heat sink product.

Once again we begin the ESM with a lumped model of the system. A CPU cooling process can be approximated as an electric circuit [17,27]. The lumped model of the CPU cooling process with heat sinks is depicted in Fig. 10. In the figure, h and k are unknown effective thermal convection and conduction coefficients, while A and A_c denote the effective convection and conduction areas of heat sinks, respectively. A resistor array is used to represent the CPU. The lumped model is built with the assumptions that (1) heat transfer from the sides and the bottom surface of the heat source (i.e., CPU) is negligible, (2) the contact thermal resistance is negligible, and (3) the thermal conductivity is not dependent on temperature. It should be noted that, although the heat sink cooling process appears at first glance to be a single material problem, the phenomenon is affected by two main physical components, viz. the thermal boundary layer and the heat sink. Hence the lumped ESM is used to predict product performance.

From Fig. 10 and the above assumptions, the surface temperature of the resistor array with the generic DuraForm heat sink (model specimen) can be represented as

$$T_{\mathrm{ms}} = q_m(R_h + R_k) + T_\infty \tag{14}$$

where $R_h = 1/hA$ and $R_k = L/kA_c$ are unknown convection and conduction thermal resistances, respectively, q is the unknown heat transfer rate, and $T_\infty = 19°\mathrm{C}$ is the ambient temperature. The temperature of the model, product specimen, and product can now be represented as

$$\begin{aligned} T_m &= q_m(\phi_h R_h + \phi_k R_k) + T_\infty, \\ T_{\mathrm{ps}} &= q_p(\lambda_h R_h + \lambda_k R_k) + T_\infty, \\ T_p &= q_p(\phi_k \lambda_h R_h + \phi_k \lambda_k R_k) + T_\infty. \end{aligned} \tag{15}$$

In Eq. (15), λ_h and λ_k are scale factors that represent the variation of R_h and R_k under material and boundary condition changes (with no change in the heat sink geometry). In contrast, ϕ_h and ϕ_k are form factors that represent the variation of R_h and R_k under purely geometry changes.

Unlike the archery bow example, more information is needed to represent T_p for the heat sink as a function of T_m, T_{ms}, T_{ps} since the number of unknowns ($T_p, \phi_h, \phi_k, \lambda_h, \lambda_k, R_h, R_k$) exceeds the number of given equations. In this example, we measure T^* (the temperature at the top of the heat sink, as shown in Fig. 10) experimentally to estimate T_p from T_m, T_{ms}, T_{ps}, T_m^*, T_{ms}^*, and T_{ps}^*.

By submodeling the convection process, the following equations can be derived:

$$T_{\mathrm{ms}}^* - T_\infty = q_m R_h, \quad T_m^* - T_\infty = q_m \phi_h R_h, \quad T_{\mathrm{ps}}^* - T_\infty = q_p \lambda_h R_h. \tag{16}$$

Similarly, by focusing on the conduction process, the following equations can be derived:

$$T_{\mathrm{ms}} - T_{\mathrm{ms}}^* = q_m R_k, \quad T_m - T_m^* = q_m \phi_k R_k, \quad T_{\mathrm{ps}} - T_{\mathrm{ps}}^* = q_p \lambda_k R_k. \tag{17}$$

From the above six additional equations, the following unknown form factors can be derived:

$$\phi_h = \frac{T_m^* - T_\infty}{T_{\mathrm{ms}}^* - T_\infty}, \quad \phi_k = \frac{T_m - T_m^*}{T_{ms} - T_{\mathrm{ms}}^*}. \tag{18}$$

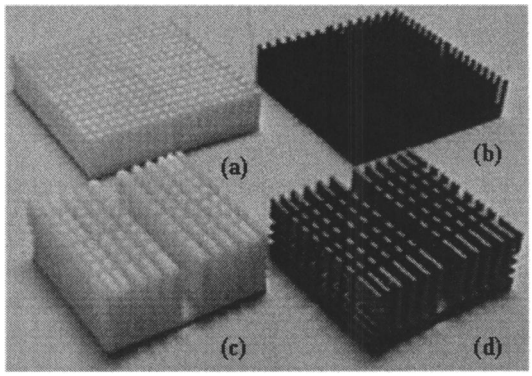

(a) Top Left: Durafom Generic Heat Sink (Model Specimen)
(b) Top Right: Aluminum Generic Heat Sink (Product Specimen)
(c) Bottom Left: Durafom Pentium Heat Sink (Model)
(d) Bottom Right: Aluminum Pentium Heat Sink (Product)

Fig. 11 DuraForm and aluminum heat sinks

[3]DuraForm™ is a polyamide-based powder for selective laser sintering processes.

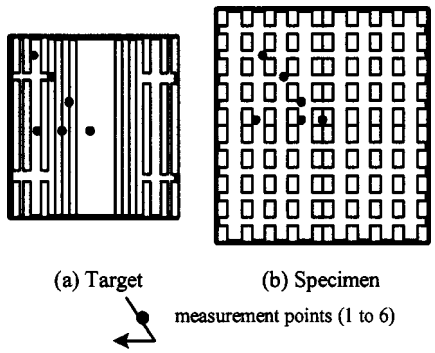

Fig. 12 Top view of heat sinks

Substituting Eqs. (16), (17), and (18) into the last of Eqs. (15) gives the ESM prediction equation for the heat sink as

$$T_p=(T_{\mathrm{ps}}^*-T_\infty)\left(\frac{T_m^*-T_\infty}{T_{\mathrm{ms}}^*-T_\infty}\right)+(T_{\mathrm{ps}}-T_{\mathrm{ps}}^*)\left(\frac{T_m-T_m^*}{T_{\mathrm{ms}}-T_{\mathrm{ms}}^*}\right)+T_\infty . \tag{19}$$

In order to predict the temperature of the aluminum CPU heat sink, as described in Eq. (19), a model and model specimen were created, and a product specimen was selected. The heat sinks used in this experiment are shown in Fig. 11. First, the aluminum CPU heat sink (with complex geometry) was established as the final product of interest. A generic aluminum heat sink (i.e., a previous version of the product with relatively simple geometry) was then selected as the product specimen. Model heat sinks were then fabricated using DuraForm in the SLS process.

Detailed top views of the targets (aluminum and DuraForm CPU heat sinks) and specimens (aluminum and DuraForm generic heat sinks) and the six chosen measurement locations are shown in Fig. 12. A resistor array composed of four power resistors was used to emulate the CPU. Figure 13 depicts the overall view of the experiment. Initially the same voltage was supplied to the resistor array for both the DuraForm and the aluminum heat sinks. However, the temperature of the resistor surface rose too high for the DuraForm heat sinks. In order to prevent thermal deformation when testing with DuraForm heat sinks, the resistor voltage was lowered and the fan voltage (and thus, fan speed) was increased for better heat dissipation. Thus the boundary conditions, as well as the material properties, were scaled for the heat sink models. Such scaling of boundary conditions is acceptable as long as the ESM assumptions described earlier are met. Table 2 shows the system parameter settings for the experiment. Table 2 also shows the steady-state temperatures of the top of the model, model specimen, and product specimen heat sinks as determined experimentally.

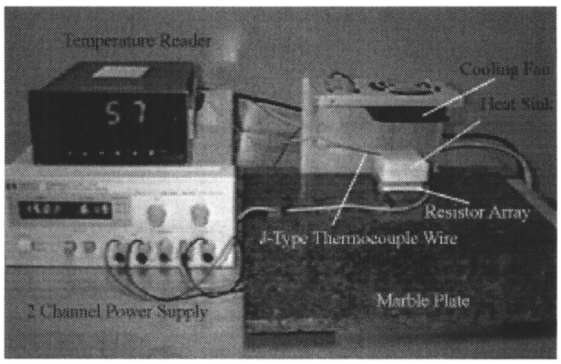

Fig. 13 Overview of CPU cooling experiment

Table 2 Model and product systems for CPU cooling test

Test conditions	Model system	Product system
Resistor voltage (V_r)	15 V	20 V
Cooling fan voltage (V_f)	20 V	15 V
Heat sink material	DuraForm	Aluminum
Temperature at heat sink top	$T_m^*=54°\mathrm{C}$, $T_{\mathrm{ms}}^*=65°\mathrm{C}$	$T_{\mathrm{ps}}^*=25°\mathrm{C}$

Figure 14 shows the measured steady-state temperature at the six selected points of the resistor surface with both DuraForm and aluminum heat sinks. The generic aluminum heat sink shows better cooling performance (due to its larger size) than the aluminum CPU heat sink. The DuraForm heat sinks increased the surface temperature by working as heat insulators rather than conductors. It is interesting to note the opposite trends in the two plots: The generic aluminum heat sink is the better conductor, and the DuraForm version of the generic heat sink is the better insulator. One can perceive the difficulty in traditional scale testing with such qualitative dissimilarity.

The temperatures at the six points of the resistor array surface with the aluminum CPU heat sink are predicted by using Eq. (19) and the measurements shown in Table 2 and Fig. 14. The mea-

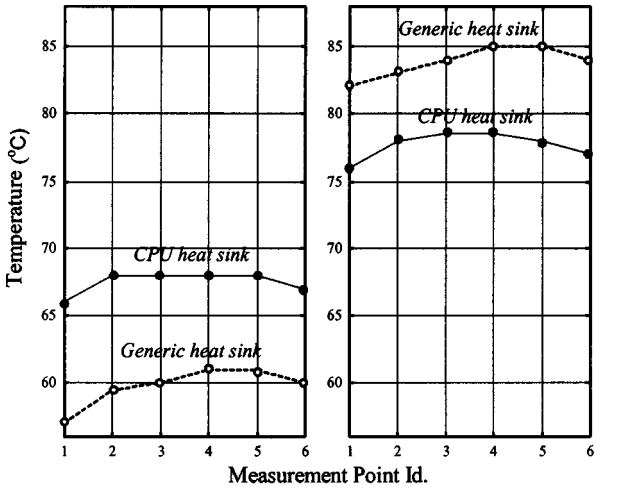

Fig. 14 Measured surface temperature

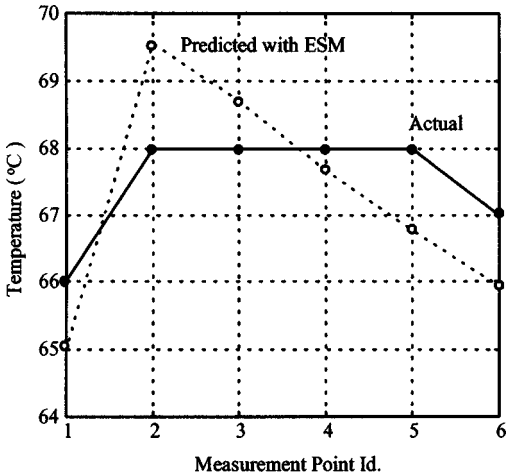

Fig. 15 Predicted surface temperature

sured temperature of the resistor array surface with the aluminum CPU heat sink is used to verify the predicted results. Figure 15 compares the predicted and actual temperatures of the resistor array surface with the aluminum CPU heat sink. The prediction error is within 2°C overall. The testing results demonstrate the accuracy of the lumped ESM.

It is worthwhile to note that the temperature of the CPU (resistor array) surface with the aluminum heat sink was predicted with the ESM without knowing such system parameters as thermal conductivity or convection coefficients explicitly. The TSM, on the other hand, requires a priori knowledge of such parameters in order to develop proper scaling factors. Due to the distinctive thermal conductivity and heat capacitance of DuraForm and aluminum relative to air, even qualitative temperature prediction is difficult. Through the lumped ESM, however, we successfully correlated the steady-state thermal behavior of heat sink systems with highly distorted configurations.

Conclusions

The concept of the ESM involves deriving similarity transformations by employing a specimen pair. The lumped ESM presented in this paper is a specific approach to embody the concept of the ESM. The ESM concept can be adapted to different situations with different details, depending on available physical insights [28–30].

The ESM can be used for a wide array of problems, but is especially suited for products that have geometric or material requirements that result in high fabrication costs. The ESM is also well suited for products for which a product specimen already exists (such as in product redesign) or for which the product specimen can be easily fabricated. Application of the ESM also has certain limitations. For example, an implicit requirement of the ESM is that geometric simplifications used for the specimen pair, as well as material changes used in the models, must not alter the overall functional behavior of the product (e.g., electromagnetic characteristics of a product cannot be predicted with a Duraform model since Duraform does not conduct electricity). This inherent condition of the ESM requires a basic knowledge of the effect of various system parameters on product performance, although it is still much less than that needed for the TSM. In addition, the lumped ESM requires that appropriate lumped models can be created for the system of interest. The creation of an appropriate lumped model may be difficult in some cases. Care should be taken when creating lumped models to include such effects as contact thermal resistances when necessary. Various spatio-temporal measurement points may be used to validate modeling assumptions.

In parallel with our efforts to construct improved similarity transformations, we are also working on error measures to provide confidence in both TSM and ESM results [31]. Through the error measures and advances in the ESM, we expect to dramatically improve the performance of product design and development processes in very broad problem domains.

Acknowledgments

The research reported in this document was made possible, in part, by a Young Investigator Award from the National Science Foundation. The authors also wish to acknowledge the support of the Ford Motor Company, Texas Instruments, DTM Corporation, and the UT June and Gene Gillis Endowed Faculty Fellowship. Any opinions, findings, or recommendations are those of the authors and do not necessarily reflect the views of the sponsors.

References

[1] Pahl, G., and Beitz, W., 1984, *Engineering Design: A Systematic Approach*, The Design Council, Springer-Verlag, London.
[2] Ullman, D., 1992, *The Mechanical Design Process*, McGraw-Hill, New York.
[3] Otto, K., and Wood, K., 2000, *Product Design*, Prentice-Hall, New York.
[4] Holmes, M. F., 1984, ''Machine Dynamics, The Need for Greater Productivity,'' in Research Needs, K. N. Reid, ed., Mechanical Systems, ASME, NY, pp. 140–159.
[5] Ulrich, K. T., and Eppinger, S. D., 1995, *Product Design and Development*, McGraw-Hill, New York.
[6] Jacobs, P. F., 1992, *Rapid Prototyping and Manufacturing: Fundamentals of StereoLithography*, Society of Manufacturing Engineers, McGraw-Hill, New York.
[7] Aubin, R. F., 1994, ''A World Wide Assessment of Rapid Prototyping Technologies,'' *Proceedings of Solid Freeform Fabrication Symposium*, August, University of Texas, Austin, TX, pp. 118–145.
[8] Dornfield, W. H., 1995, ''Direct Dynamic Testing of Scaled Stereolithographic Models,'' Sound Vib., , pp. 12–17.
[9] O'Reilly, S. B., 1993, ''FFF at Ford Motor Company,'' *Proceedings of the 1993 SFF Symposium*, University of Texas, Austin, TX, pp. 168–177.
[10] Rodriquez, J. F., Thomas, J. P., and Renaud, J. E., 2003, ''Design of Fused-Deposition ABS Components for Stiffness and Strength,'' ASME J. Mech. Des., **125**, pp. 545–551.
[11] Wall, M. B., Ulrich, K. T., and Flowers, W. C. 1991, ''Making Sense of Prototyping Technologies for Product Design,'' *Proceeding of ASME 3rd International Conference on Design Theory and Methodology*, Vol. DE-31, ASME, New York, pp. 157–164.
[12] Bridgman, P. W., 1937, *Dimensional Analysis*, Yale University Press, New Haven.
[13] Langhaar, H. L., 1951, *Dimensional Analysis and Theory of Models*, Wiley, New York.
[14] Sedov, L. I., 1959, *Similarity and Dimensional Methods in Mechanics*, Academic Press, New York.
[15] Szucs, E., 1980, *Similitude and Modeling*, Elsevier Scientific, New York.
[16] Baker, W. E., Westine, P. S., and Dodge, F. T., 1991, *Similarity Methods and Engineering Dynamics: Theory and Practice of Scale Modeling*, Elsevier, New York.
[17] Kline, S. J., 1965, *Similitude and Approximate Theory*, McGraw-Hill, New York.
[18] Bluman, G. W., and Kumei, S., 1989, *Symmetries and Differential Equations*, Springer-Verlag, New York.
[19] Barr, D., 1984, ''Consolidation of Basics of Dimensional Analysis,'' J. Eng. Mech., **10(9)**, pp. 1357–1375.
[20] Murphy, G., 1950, *Similitude in Engineering*, The Ronald Press Company, New York.
[21] Intel, 1998, ''Thermal Management,'' http://support.intel.com/support/processors/pentiumii/1793.htm
[22] Nadworny, E. B., 1995, ''High Power CPU Cooling Experiment,'' *Proceedings of the Computers in Engineering Conference and the Engineering Database Symposium*, ASME, Boston, MA, pp. 1057–1066.
[23] Fisher, T. S. et al., 1997, ''Analysis and Optimization of a Natural Draft Heat Sink System,'' IEEE Trans. Compon., Packag. Manuf. Technol., Part A, **20(2)**, pp. 111–119.
[24] Linton, R. L., and Agonafer, D., 1995, ''Coarse and Detailed CFD Modeling of a Finned Heat Sink,'' *Proceedings of the 4th Intersociety Conference on Thermal and Thermo Mechanical Phenomena in Electronic Systems*, Washington, DC.
[25] Beaman, J. J., Barlow, J. W., Bourell, D. L., Crawford, R. H., Marcus, H. L., and McAlea, K. P., 1997, *Solid Freeform Fabrication: A New Direction in Manufacturing*, Kluwer, Norwell.
[26] Conley, J. G., and Marcus, H. L., 1997, ''Rapid Prototyping and Solid Free Form Fabrication,'' ASME J. Manuf. Sci. Eng., **119**, pp. 811–816.
[27] Incropera, F. P., 1981, *Fundamentals of Heat Transfer*, Wiley, New York.
[28] Cho, U., and Wood, K. L. 1997, ''Empirical Similitude Method for the Functional Test With Rapid Prototypes,'' *Proceedings of the 1997 Solid Freeform Fabrication Symposium*, University of Texas, Austin, TX, pp. 559–567.
[29] Cho, U., Wood, K. L., and Crawford, R. H., 1998(a), ''Online Functional Test With Rapid Prototypes: A Novel Empirical Similarity Method,'' Rapid Prototyping Journal, **4(3)**, pp. 128–138.
[30] Cho, U., Wood, K. L., and Crawford, R. H., 1998(b), ''Novel Empirical Similarity Method for the Reliable Product Test With Rapid Prototypes,'' *Proceedings of the 1998 ASME DETC*, number 98-DETC/DAC-5605, Atlanta, GA, ASME, New York.
[31] Cho, U., Wood, K. L., and Crawford, R. H., 1999, ''Error Measures for Functional Product Testing,'' *Proceedings of the 1999 ASME DETC*, number 99-DETC/DFM-8913, Las Vegas, NV, ASME, New York.